Int J Fract (2022) 234:297–311
https://doi.org/10.1007/s10704-021-00602-2

ORIGINAL PAPER

A three-dimensional non-local lattice bond model for fracturing behavior prediction in brittle solids

Liang Fu · Xiao-Ping Zhou · Filippo Berto

Received: 26 June 2021 / Accepted: 20 October 2021 / Published online: 10 January 2022

Abstract In this paper, a 3D non-local lattice bond model is proposed to model fracturing behaviors of materials. First, the formulations and detailed derivation for three-dimensional non-local lattice bond models are obtained by comparing the strain energy stored in a discrete lattice with the classical continuum strain energy. Then, the capabilities of three-dimensional non-local lattice bond models are verified using benchmarks. To further assess the performance of the non-local lattice bond model, fracturing behaviors in brittle solids are predicted. Compared with the previous numerical results, the proposed model demonstrates better performances, which are more consistent with the experimental observations.

Keywords 3D non-local lattice bond model · Fracturing behaviors · Brittle solid

L. Fu · X.-P. Zhou (✉)
School of Civil Engineering, Chongqing University, Chongqing 400045, People's Republic of China
e-mail: cqxpzhou@hotmail.com; zhouxiaoping@cqu.edu.cn

F. Berto
Department of Mechanical Engineering, Norwegian University of Science and Technology, 7491 Trondheim, Norway

1 Introduction

Understanding the characteristics of fracture evolution is of great importance in solid mechanics (Wang et al. 2018a,b; Zhou et al. 2018). The numerical method plays a key role in studying the fracture evolution, which has attracted researchers in different disciplines in past decades because it saves money and time (Yang et al. 2016; Zhou and Shou 2016). Up to now, numerous numerical methods have been performed to address fracture behaviors, which mainly include the continuum-based methods and the discontinuous methods (Cusatis et al. 2003; Wang et al. 2018a,b; Zhao et al. 2019).

Nowadays, continuum-based methods, i.e., the Finite Element Method, are investigated extensively in practical engineering and have been used to address three-dimensional fracture evolution in the past decades (Zienkiewicz and Taylor 2000). However, the generation and refinement of the mesh in FEM should be carefully considered. In addition, it should handle the difficulties related to the singularity of crack tips during fracture simulation carefully. Especially, when these problems are in the three-dimensional case, the difficulties become more apparent. The eXtended Finite Element Method (XFEM) (Belytschko et al. 2009) is developed from the classical FEM, which makes implementing the required prior knowledge of mesh matching on crack path easier and provides a less computationally expensive scheme (Zeng et al. 2013; Yu et al. 2015; Zhou et al.

2020a,b). However, XFEM does not suitably provide a holistic and comprehensive external criterion for fracture evolution.

As alternatives, a great number of discontinuous methods are more often used to solve singularity related issues in dealing with fracture problems, including the Lattice Models (LM) (Ostoja-Starzewski 2002), the Discrete Element Method (DEM) (Cundall and Strack 1979), the Numerical Manifold Method (NMM) (Yang et al. 2016) and the Discontinuous Deformation Analysis (DDA) (Chen and Wu 2018). In the discontinuous methods, materials are discretized into a set of discrete elements, which are connected by different types of interactions. The fracture evolution is implemented by terminating the interaction between the elements. In spite of the advantages of crack simulation, the discontinuous methods have also some limitations, such as free surface effects and fixed Poisson's ratio (Zhang and Ge 2007). Therefore, in the present paper, the 3D non-local lattice bond model is proposed to eliminate the limitation of fixed Poisson's ratio.

In 1941, Hrennikoff (1941) developed lattice model to simulate the mechanical behaviors of materials, in which materials were considered an assemblage of lattices connected by springs. The main advantages of lattice model are that the singularity related problems are avoided and no additional fracture criterion is required. Since then, the lattice model had been successfully developed by many scholars (Zubelewicz and Bažant 1987; Zhao 2017; Zhou et al. 2020a,b). A well-known limitation of the lattice model is the problem of fixed Poisson's ratio only if normal bonds transmitting central forces are considered. To solve the issue, numerous models are developed by introducing local non-central interactions. Kawai (1978) incorporated the concept of shear bond into the lattice model to eliminate the limitation of fixed Poisson's ratio. After that, Griffiths (2001) developed this lattice model in more detail. Caldarelli et al. (1999) limited the rotational freedom of bonds by considering a non-central two-body interaction. Lilliu and van Mier (2003) presented the lattice beam model, LBM, to consider bending stiffness of beam in shear deformation. Another method to solve the above problem is to consider nonlocal interaction terms. Grassl et al. (2006) employed the non-local irregular truss with plane strain assumption, and successfully simulated the fracture evolution of brittle materials. Zhao et al. (2019) numerically investigated the fracture behavior by incorporating non-local potential in the lattice model. Zhou et al. (2021) developed a novol two-dimensional non-local lattice bond model (NLBM) for crack behaviors in rock materials.

In the previous work conducted by Zhou et al. (2021) the material was discretized into regular hexagonal lattices, which made it difficult to generalize the model to three-dimensional case. In the present paper, the two-dimensional model is extended to three-dimensional case by discretizing materials into regular cubic lattice. By introduction of the non-local tangential bonds perpendicular to the normal bonds between two lattices, the fixed Poisson's ratio limitation is eliminated. Furthermore, by introducing the concept of force density inspired by peridynamics (Silling et al. 2007), the proposed model can easily incorporate intermolecular and surface forces into the constitutive model, which is very attractive for certain applications (Zhou et al. 2021). The capabilities of three-dimensional non-local lattice bond model are demonstrated by using various benchmarks, including elastic and fracture problems.

The present paper is organized as follows: in Sect. 2, the formulations and detailed derivation for three-dimensional non-local lattice bond model are obtained. Several benchmarks are conducted to verify the capabilities of the proposed model in Sect. 3. Conclusions are drawn in Sect. 4.

2 The non-local lattice bond model

In both the classical lattice spring model and bond-based peridynamics, materials are discretized into a set of discrete elements, which are connected by normal springs or bonds. However, in classical lattice spring model, the number and the vector of the springs with a lattice are determined a priori. Moreover, the connection between microstructure parameters and macrostructure parameters are obtained by comparing the strain energy stored in a lattice with the classical continuum strain energy. Different from the classical lattice spring model, the bonds are randomly distributed and the non-local concept is used to solve the crack path preference problems in bond-based peridynamics. In non-local lattice bond models, solids are composed of regularly packed lattices, which are connected via normal and tangential bonds. The

proposed model, in which the rotation freedom of two lattices is restricted by the tangential bonds, is different from classical lattice spring model. It is also different from the bond-based peridynamics, in which the bonds are randomly distributed.

To solve the Poisson's ratio problems caused by considering only the normal bonds transmitting central forces, the materials are discretized into a new microstructure in the present paper. As shown in Fig. 1a, in the three-dimensional case, the interaction between two lattices can be divided into two parts including a normal bond and three tangential bonds. The normal bond transmits normal force which is related to the normal displacement, and these three tangential bonds transmit shear forces which are related to the rotation of normal bond along three coordinate axes. Similar to the three-dimensional case, the interaction between two lattices can be divided into two parts including a normal bond and two tangential bonds in the two-dimensional case, as shown in Fig. 1b. Furthermore, the essence of this proposed model is to make the discrete lattices equal to the continuum element. The energy potentials of this proposed model are derived from the equivalent discrete lattices, as shown in Fig. 2.

2.1 A general derivation of the NLBM

As shown in Fig. 1, the energy potential w stored in bonds between each pair of lattices can be describe as the stretch energy potential w_ℓ and rotation energy potential w_β. In the three-dimensional case, unit orientation vector of the normal bond is $n_i = (\sin\theta\cos\varphi, \sin\theta\sin\varphi, \cos\theta)$ in the Cartesian coordinate system, as shown in Fig. 2a. Its length change can be written as $\delta l_{IJ} = l_0 n_i \varepsilon_{ij} n_j$, where l_0 is the bond length before deformation and ε_{ij} is the strain tensor. Hence, the stretch energy potential of a normal bond is:

$$w_{\ell j} = \frac{1}{2} k_n (\delta l_{IJ})^2 = \frac{1}{2} k_n (l_0 n_i \varepsilon_{ij} n_j)^2 \tag{1}$$

where k_n is the stretch stiffness parameter.

Furthermore, the stretch energy potential w_ℓ stored in a unit lattice associated with N normal bonds can be expressed as:

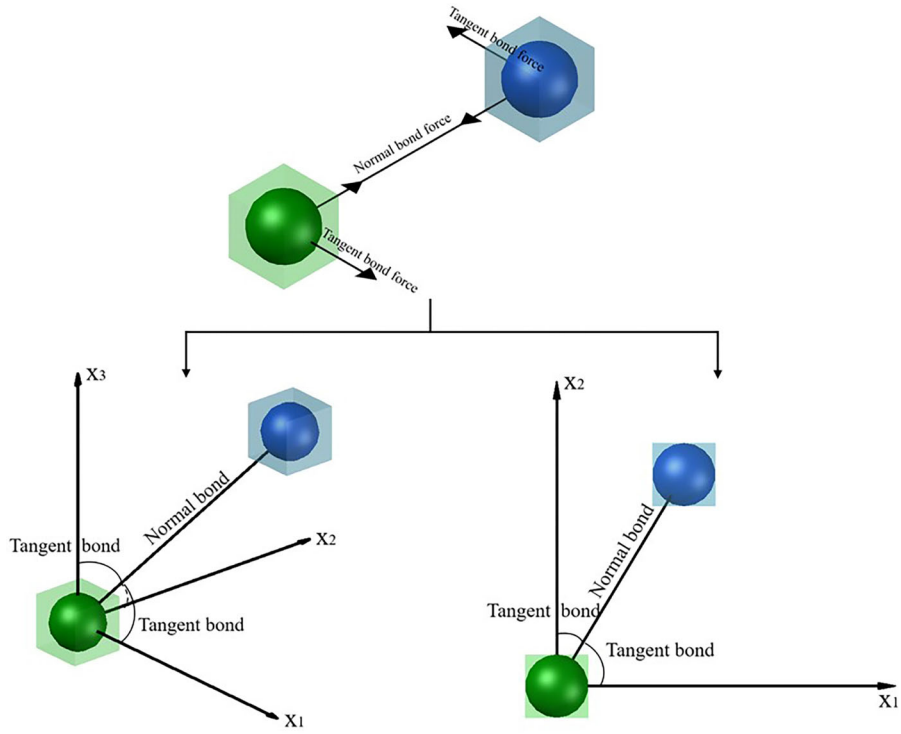

(a) The three-dimensional case **(b)** The two-dimensional case

Fig. 1 The microstructure of the non-local lattice bond model

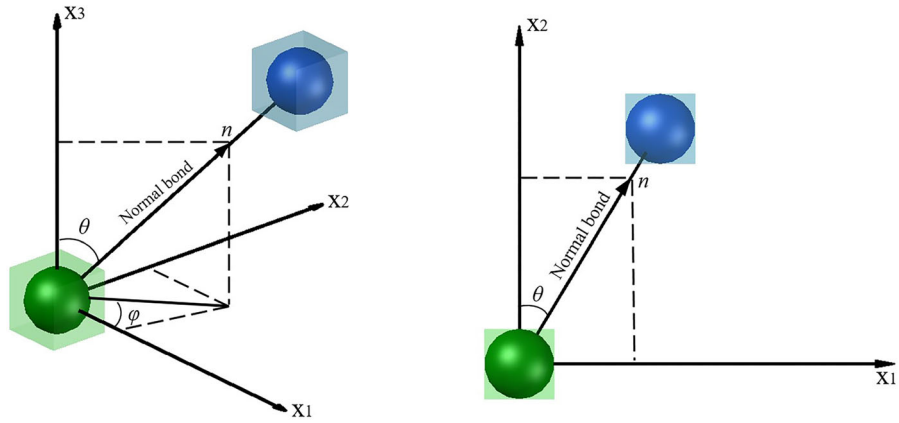

Fig. 2 Orientation and rotation vector of a normal bond

(a) The three-dimensional case **(b)** The two-dimensional case

$$w_\ell = \sum_{j=1}^{n} w_{\ell j} = \frac{1}{2} k_n \sum_{j=1}^{n} \left(l_0 n_i \varepsilon_{ij} n_j\right)^2 \tag{2}$$

Based on the work by Zhang and Ge (2006), the rotation angle β can be divided into three parts along the three coordinate axes in the case of small deformation:

$$\begin{aligned} \beta_1 &= n_i \varepsilon_{ij} \lambda_j' \\ \beta_2 &= n_i \varepsilon_{ij} \lambda_j'' \\ \beta_3 &= n_i \varepsilon_{ij} \lambda_j''' \end{aligned} \tag{3}$$

where λ is the unit vector perpendicular to n and can be written as:

$$\begin{aligned} \lambda_j' &= \left(\sin^2\theta\sin^2\varphi + \cos^2\theta, -\sin^2\theta\cos\varphi\sin\varphi, -\sin\theta\cos\varphi\cos\theta\right) \\ \lambda_j'' &= \left(-\sin^2\theta\cos\varphi\sin\varphi, \sin^2\theta\cos^2\varphi + \cos^2\theta, -\sin\theta\sin\varphi\cos\theta\right) \\ \lambda_j''' &= \left(-\sin\theta\cos\varphi\cos\theta, -\sin\theta\sin\varphi\cos\theta, \sin^2\theta\right) \end{aligned} \tag{4}$$

Therefore, the rotation energy potential w_β stored in a lattice associated with N normal bonds can be derived as:

$$w_\beta = \frac{1}{2} k_s \sum_{j=1}^{n} \left[\left(n_i \varepsilon_{ij} \lambda_j'\right)^2 + \left(n_i \varepsilon_{ij} \lambda_j''\right)^2 + \left(n_i \varepsilon_{ij} \lambda_j'''\right)^2 \right] \tag{5}$$

where k_s is the rotation stiffness parameter.

The energy potential of a lattice can be expressed by the stretch energy potential and rotation energy potential as:

$$w = w_\ell + w_\beta \tag{6}$$

The strain energy density can be written as:

$$\begin{aligned} W^{3D} = &\frac{1}{2} \sum_{j=1}^{n} \frac{1}{2} k_n \left(l_0 n_i \varepsilon_{ij} n_j\right)^2 V_j \\ &+ \frac{1}{2} \sum_{j=1}^{n} \frac{1}{2} k_s \left[\left(n_i \varepsilon_{ij} \lambda_j'\right)^2 + \left(n_i \varepsilon_{ij} \lambda_j''\right)^2 + \left(n_i \varepsilon_{ij} \lambda_j'''\right)^2 \right] V_j \end{aligned} \tag{7}$$

where V_j is the volume of the unit lattice and $V_j = 8R^3$.

From Eq. (7), the stress tensor is expressed as:

$$\sigma_{ij} = \frac{\partial W^{3D}}{\partial \varepsilon_{ij}} \tag{8}$$

Figure 3a illustrates a lattice containing 18 related normal vector directions in the three-dimensional case. These 18 normal vectors can be divided into two kinds of neighbors and the normal vectors are listed in Table 1. From Eq. (7), the strain energy density in the three-dimensional case is given as:

$$\begin{aligned} W^{3D} = &\left(16R^5 k_{n1} + 32R^5 k_{n2} + 4R^3 k_{s2}\right)\left(\varepsilon_{11}^2 + \varepsilon_{22}^2 + \varepsilon_{33}^2\right) \\ &+ \left(16R^5 k_{n2} + 2R^3 k_{s1} + 2R^3 k_{s2}\right)\left(\gamma_{12}^2 + \gamma_{13}^2 + \gamma_{23}^2\right) \\ &+ \left(32R^5 k_{n2} - 4R^3 k_{s2}\right)\left(\varepsilon_{11}\varepsilon_{22} + \varepsilon_{11}\varepsilon_{33} + \varepsilon_{22}\varepsilon_{33}\right) \end{aligned} \tag{9}$$

where k_{n1} and k_{s1} are the stiffness parameters for the 1st-nearest-neighbor and k_{n2} and k_{s2} are the stiffness parameters for the 2nd-nearest-neighbor.

It is assumed that k_{s1} and k_{s2} are equal to k_s. From Eq. (9), each of strain terms is expressed as:

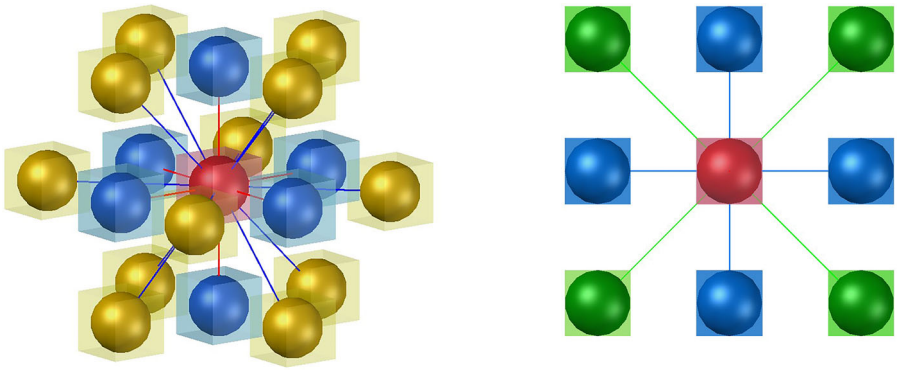

(a) The three-dimensional case **(b)** The two-dimensional case

Fig. 3 The connecting relationship of the center lattice

Table 1 The normal vectors in the three-dimensional case

Neighbors 1					
n_1	n_2	n_3	n_4	n_5	n_6
$(1,0,0)$	$(0,1,0)$	$(0,0,1)$	$(-1,0,0)$	$(0,-1,0)$	$(0,0,-1)$
Neighbors 2					
n_7	n_8	n_9	n_{10}		
$1/\sqrt{2}(1,1,0)$	$1/\sqrt{2}(-1,1,0)$	$1/\sqrt{2}(-1,-1,0)$	$1/\sqrt{2}(1,-1,0)$		
n_{11}	n_{12}	n_{13}	n_{14}		
$1/\sqrt{2}(1,0,1)$	$1/\sqrt{2}(1,0,-1)$	$1/\sqrt{2}(-1,0,-1)$	$1/\sqrt{2}(1,0,-1)$		
n_{15}	n_{16}	n_{17}	n_{18}		
$1/\sqrt{2}(0,1,1)$	$1/\sqrt{2}(0,-1,1)$	$1/\sqrt{2}(0,-1,-1)$	$1/\sqrt{2}(0,1,-1)$		

$$
\begin{aligned}
\sigma_{11} &= \left(32R^5k_{n1} + 64R^5k_{n2} + 8R^3k_s\right)\varepsilon_{11} \\
&\quad + \left(32R^5k_{n2} - 4R^3k_s\right)(\varepsilon_{22} + \varepsilon_{33}) \\
\sigma_{22} &= \left(32R^5k_{n1} + 64R^5k_{n2} + 8R^3k_s\right)\varepsilon_{22} \\
&\quad + \left(32R^5k_{n2} - 4R^3k_s\right)(\varepsilon_{11} + \varepsilon_{33}) \\
\sigma_{33} &= \left(32R^5k_{n1} + 64R^5k_{n2} + 8R^3k_s\right)\varepsilon_{33} \\
&\quad + \left(32R^5k_{n2} - 4R^3k_s\right)(\varepsilon_{11} + \varepsilon_{22}) \\
\tau_{12} &= \left(32R^5k_{n2} + 8R^3k_s\right)\gamma_{12} \\
\tau_{23} &= \left(32R^5k_{n2} + 8R^3k_s\right)\gamma_{23} \\
\tau_{13} &= \left(32R^5k_{n2} + 8R^3k_s\right)\gamma_{13}
\end{aligned}
\tag{10}
$$

In the three-dimensional case, the Hooke's law is given by:

$$
\begin{aligned}
\sigma_{11} &= \frac{E(1-v)}{(1+v)(1-2v)}\left(\varepsilon_{11} + \frac{v}{1-v}\varepsilon_{22} + \frac{v}{1-v}\varepsilon_{33}\right) \\
\sigma_{22} &= \frac{E(1-v)}{(1+v)(1-2v)}\left(\frac{v}{1-v}\varepsilon_{11} + \varepsilon_{22} + \frac{v}{1-v}\varepsilon_{33}\right) \\
\sigma_{33} &= \frac{E(1-v)}{(1+v)(1-2v)}\left(\frac{v}{1-v}\varepsilon_{11} + \frac{v}{1-v}\varepsilon_{22} + \varepsilon_{33}\right) \\
\tau_{12} &= \frac{E}{2(1+v)}\gamma_{12} \\
\tau_{23} &= \frac{E}{2(1+v)}\gamma_{23} \\
\tau_{13} &= \frac{E}{2(1+v)}\gamma_{13}
\end{aligned}
\tag{11}
$$

By comparing Eqs. (10) with (11), the relationship among stiffness parameters k_{n1} k_{n2} and k_s and material constants, i.e. Young's modulus E and Poisson's ratio v can be solved as:

$$\begin{aligned} k_{n1} &= \frac{E(1-v)}{96R^5(1+v)(1-2v)} \\ k_{n2} &= \frac{E(1+2v)}{192R^5(1+v)(1-2v)} \\ k_s &= \frac{E(1-4v)}{24R^3(1+v)(1-2v)} \end{aligned} \tag{12}$$

where the units for the two stretch stiffness parameters are $\mathrm{N/m^7}$ and the unit for the rotation stiffness is $\mathrm{N/m^5}$.

When the stiffness parameters k_{n1} k_{n2} and k_s are obtained, the interaction forces include the 1st-nearest-neighbor normal bond force f_{n1}, the 2nd-nearest-neighbor normal bond force f_{n2} and the tangential bond force f_s can be calculated by:

$$\begin{aligned} f_{n1} &= k_{n1} \cdot \delta l \\ f_{n2} &= k_{n2} \cdot \delta l \\ f_s &= \frac{k_s \cdot \beta}{l_0} \end{aligned} \tag{13}$$

where the units of the two normal bond forces f_{n1} and f_{n2} and the tangential bond force f_s are $\mathrm{N/m^6}$.

In the two-dimensional case illustrated in Fig. 3b, Eq. (7) can be reduced to:

$$\begin{aligned} W^{2D} = &\frac{1}{2}\sum_{j=1}^{n}\frac{1}{2}k_n\left(l_0 n_i \varepsilon_{ij} n_j\right)^2 V_j \\ &+\frac{1}{2}\sum_{j=1}^{n}\frac{1}{2}k_s\left[\left(n_i\varepsilon_{ij}\lambda_j'\right)^2+\left(n_i\varepsilon_{ij}\lambda_j''\right)^2\right]V_j \end{aligned} \tag{14}$$

where $n = (\sin\theta, \cos\theta)$, $\lambda' = (\sin\theta, -\cos\theta)$, $\lambda'' = (-\sin\theta, \cos\theta)$, V_j is equal to $4R^2h$ and the unit thickness h is constant in the follow derivations.

Similar to the three-dimensional case, 8 normal vectors contained in the two-dimensional case can also be divided into two kinds of neighbors and the normal vectors are listed in Table 2.

From Eq. (14), each of strain terms in the two-dimensional case is expressed as:

Table 2 The normal vectors for the two-dimensional case

Neighbors 1			
n_1	n_2	n_3	n_4
$(1,0)$	$(0,-1)$	$(-1,0)$	$(0,1)$
Neighbors 2			
n_5	n_6	n_7	n_8
$1/\sqrt{2}(1,-1)$	$1/\sqrt{2}(-1,-1)$	$1/\sqrt{2}(-1,1)$	$1/\sqrt{2}(1,1)$

$$\begin{aligned} \sigma_{11} &= \frac{\partial W}{\partial \varepsilon_{11}} = \left(16R^4hk_{n1} + 16R^4hk_{n2} + 4R^2hk_s\right)\varepsilon_{11} \\ &\quad + \left(16R^4hk_{n2} - 4R^2hk_s\right)\varepsilon_{22} \\ \sigma_{22} &= \frac{\partial W}{\partial \varepsilon_{22}} = \left(16R^4hk_{n1} + 16R^4hk_{n2} + 4R^2hk_s\right)\varepsilon_{22} \\ &\quad + \left(16R^4hk_{n2} - 4R^2hk_s\right)\varepsilon_{11} \\ \sigma_{12} &= \frac{\partial W}{\partial \gamma_{12}} = \left(16R^4hk_{n2} + 4R^2hk_s\right)\gamma_{12} \end{aligned} \tag{15}$$

In the plane stress case, the relationship between k_{n1}, k_{n2}, k_s and E, v can be solved as:

$$\begin{aligned} k_{n1} &= \frac{E}{32R^4h(1-v)} \\ k_{n2} &= \frac{E}{64R^4h(1-v)} \\ k_s &= \frac{E(1-3v)}{16R^2h(1-v^2)} \end{aligned} \tag{16}$$

In the plane strain case, the relationship between k_{n1}, k_{n2}, k_s and E, v can be calculated by:

$$\begin{aligned} k_{n1} &= \frac{E}{32R^4h(1+v)(1-2v)} \\ k_{n2} &= \frac{E}{64R^4h(1+v)(1-2v)} \\ k_s &= \frac{E(1-4v)}{16R^2h(1+v)(1-2v)} \end{aligned} \tag{17}$$

The bond force f_{n1}, f_{n2} and f_s can be written as:

$$\begin{aligned} f_{n1} &= k_{n1} \cdot \delta l \\ f_{n2} &= k_{n2} \cdot \delta l \\ f_s &= \frac{k_s \cdot \beta}{l_0} \end{aligned} \tag{18}$$

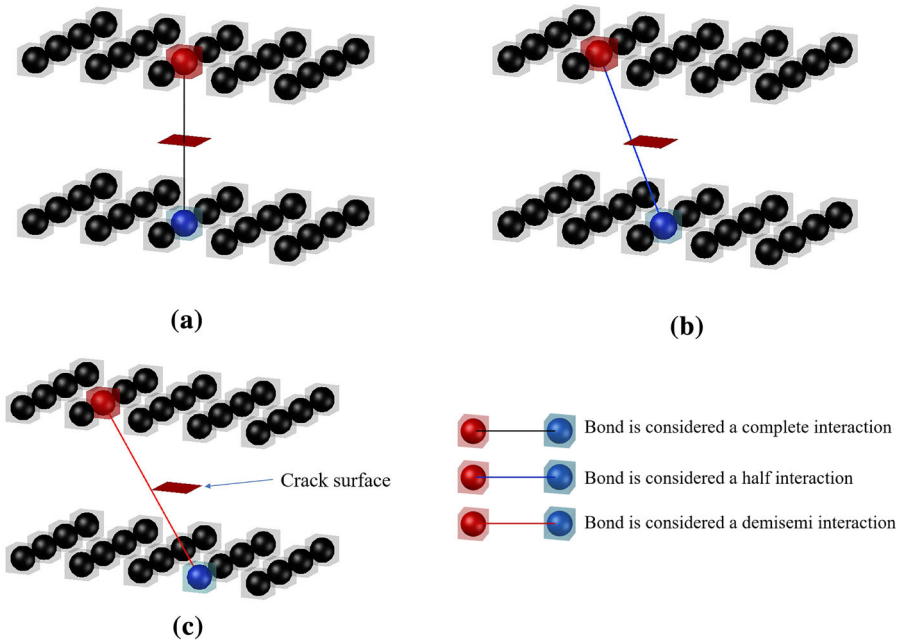

Fig. 4 Bond passing through **a** crack surface, **b** crack edges, **c** crack corners in three-dimensional case

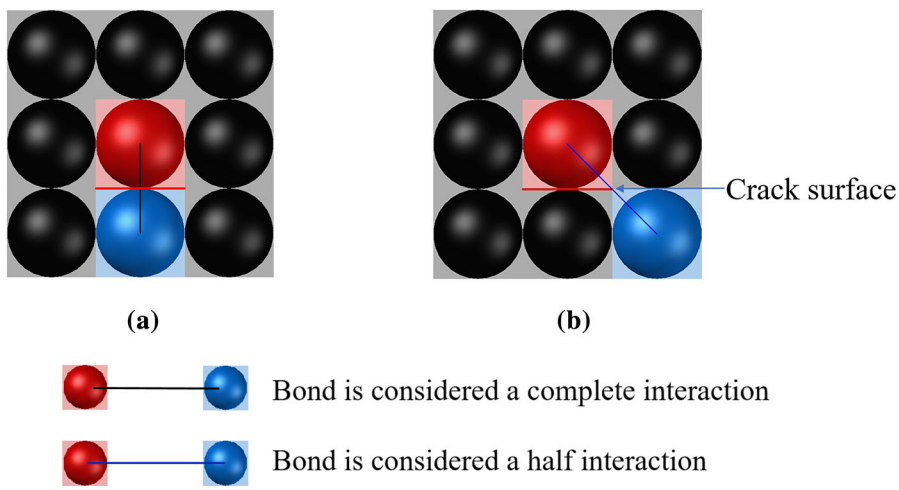

Fig. 5 Bond passing through **a** crack surface, **b** crack edges in two-dimensional case

2.2 Failure criterion

The damage prediction is implemented by terminating the interaction between lattices. The bond forces between two lattices are irreversibly eliminated when the interaction is terminated, leading to failure of bonds. The state of bonds is expressed by a scalar-valued function $\mu(x_i)$ which can be written as:

$$\mu(x_i) = \begin{cases} 1 & \text{intact} \\ 0 & \text{broken} \end{cases} \tag{19}$$

The ratio of number of broken bonds to all bonds at lattice x_i is used to define damage, which can be described as:

$$D(x_i) = 1 - \frac{\sum_1^j \mu(x_i)}{j} \tag{20}$$

In the present paper, the critical bond energy potential criterion is utilized to simulate the state of

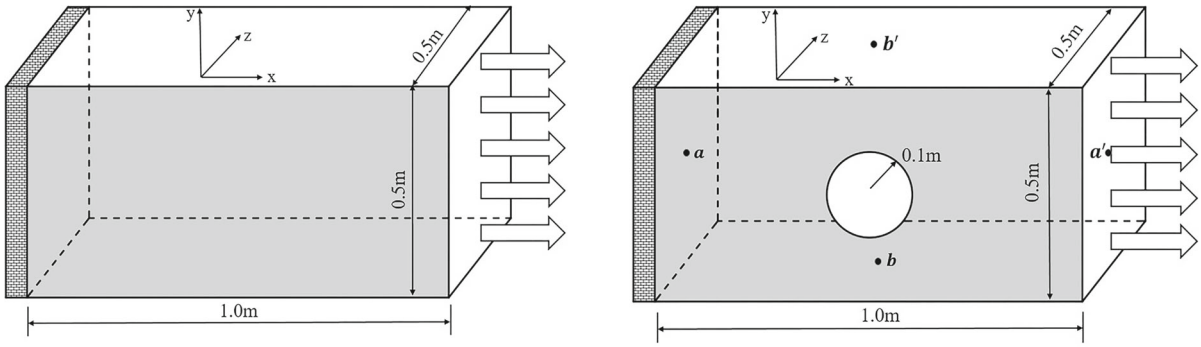

(a) a rectangular block without a hole **(b)** a rectangular block with a hole

Fig. 6 Schematic illustration of the two block

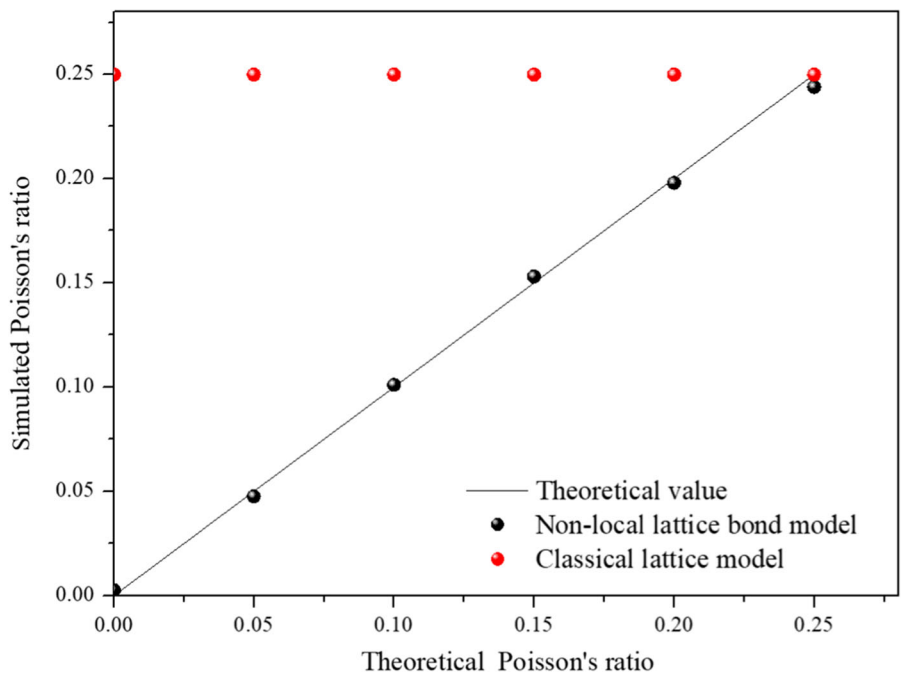

Fig. 7 The verification of Poisson's ratio

interaction (Silling and Askari 2005). If $w < w^0$, where w^0 is the critical bond energy potential value, the interaction exists and bond is intact. Otherwise, if $w > w^0$, the interaction is irreversibly eliminated and bond is broken. Inspired by Madenci and Oterkus (2014), the relationship between critical energy release rate G_c and critical bond energy potential is obtained as:

$$G_c = \frac{\sum_{j=1}^{J}\sum_{i=1}^{I}\frac{1}{2}\left(w^0_{(j)(i)} + w^0_{(i)(j)}\right)V_i V_j c_{(j)(i)}}{A} \tag{21}$$

where $c_{(j)(i)}$ is used to describe the intersecting relationship between the bond connecting lattices j and i and the crack surface A (Nguyen and Oterkus 2020). As shown in Fig. 4, in the three-dimensional case, the bond passing through crack surface is considered as complete interaction with $c_{(j)(i)} = 1$, and the bond contacting the crack edges is considered as half interaction with $c_{(j)(i)} = 1/2$, while the bond contacting the crack corners is considered as demi semi interaction with $c_{(j)(i)} = 1/4$. There exist 2 bonds passing through crack surface, 16 bonds contacting the crack edges and no bonds contacting the crack corners.

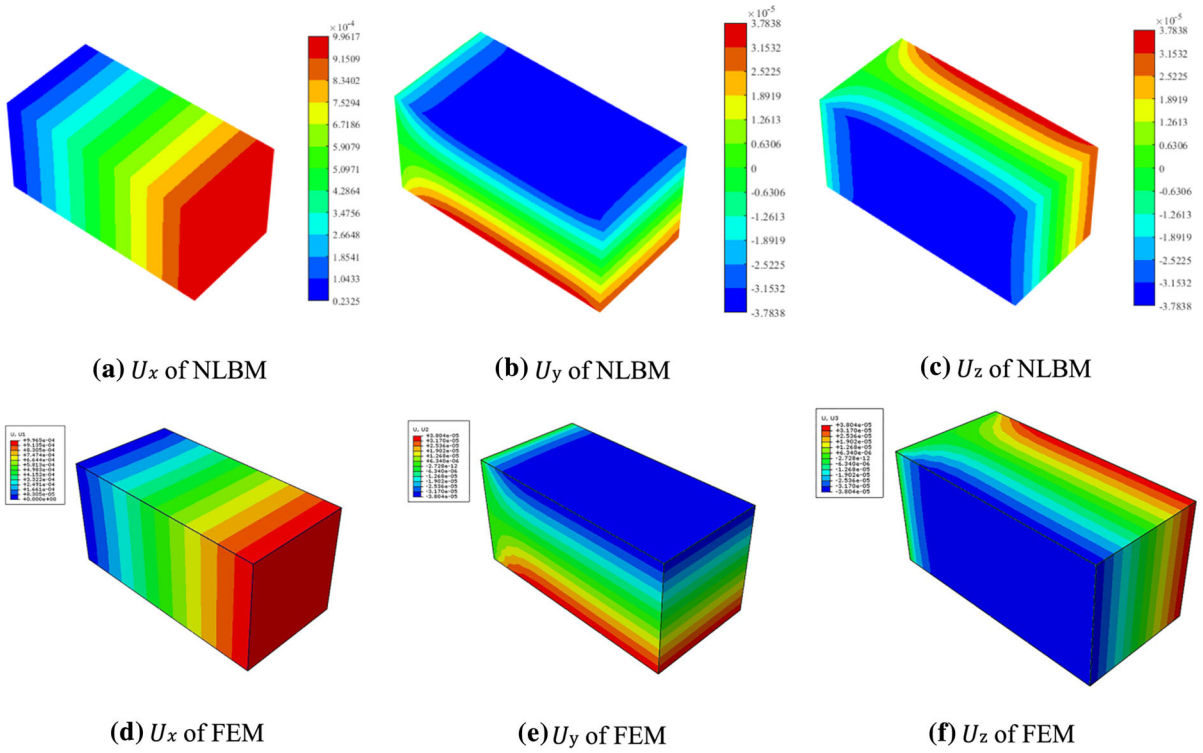

Fig. 8 Displacement contours of intact block

Therefore, total number of bonds passing through the unit crack surface is expressed as $N_c = 2 \times 1 + 16 \times \frac{1}{2} + 0 \times \frac{1}{4} = 10$.

In this paper, $w^0_{(j)(i)} = w^0_{(i)(j)} = w^0$. Moreover, by assuming that the critical energy release rate, G_c, of an unit lattice is equally distributed to each interaction passing through the crack surface, the following relation can be indicated as:

$$G_c = \frac{w^0 V_i V_j}{A} N_c \tag{22}$$

Therefore, the value of w^0 in three-dimensional case is solved as:

$$w^0_{3D} = \frac{G_c A}{V_i V_j N_c} = \frac{G_c}{160R^4} \tag{23}$$

Similarly, in two-dimensional case, there are 2 bonds passing through crack surface and 8 bonds contacting the crack edges. As shown in Fig. 5, the bond passing through crack surface is considered a complete interaction with $c_{(j)(i)} = 1$, and the bond contacting the crack edges is considered a half interaction with $c_{(j)(i)} = 1/2$. The total number of bonds passing through the unit crack surface is expressed as $N_c = 2 \times 1 + 8 \times \frac{1}{2} = 6$.

Therefore, the value of w^0 in two-dimensional case is solved as:

$$w^0_{2D} = \frac{G_c A}{V_i V_j N_c} = \frac{G_c}{48R^3 h} \tag{24}$$

3 Example of application

In this section, the elastic problems and fracture problems in three-dimensional cases and two-dimensional cases are analyzed to examine the performance of the proposed model. The results obtained by the proposed model are compared with the theoretical values, other numerical results, i.e. the finite element method (FEM), and the previous experimental observations. The explicit time integration, i.e. adaptive dynamic relaxation method, is utilized in the proposed model.

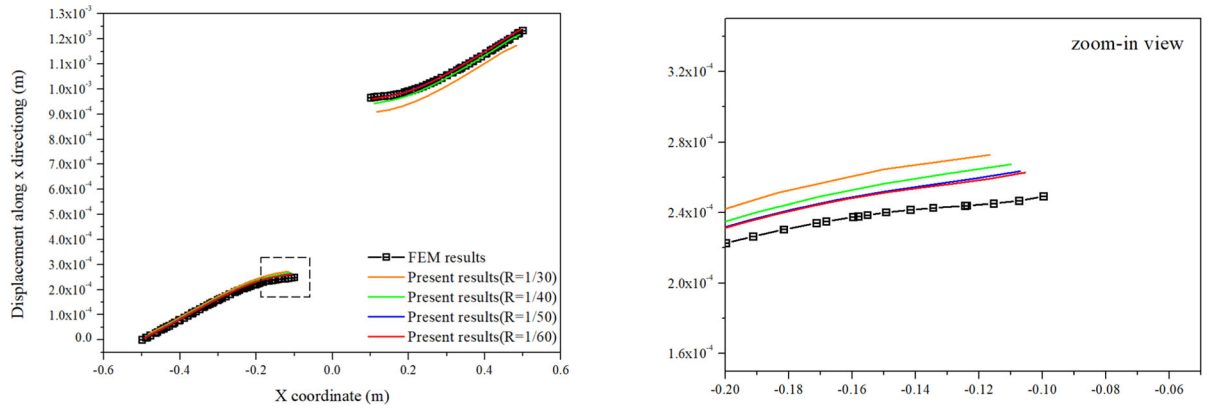

(a) Horizontal displacement

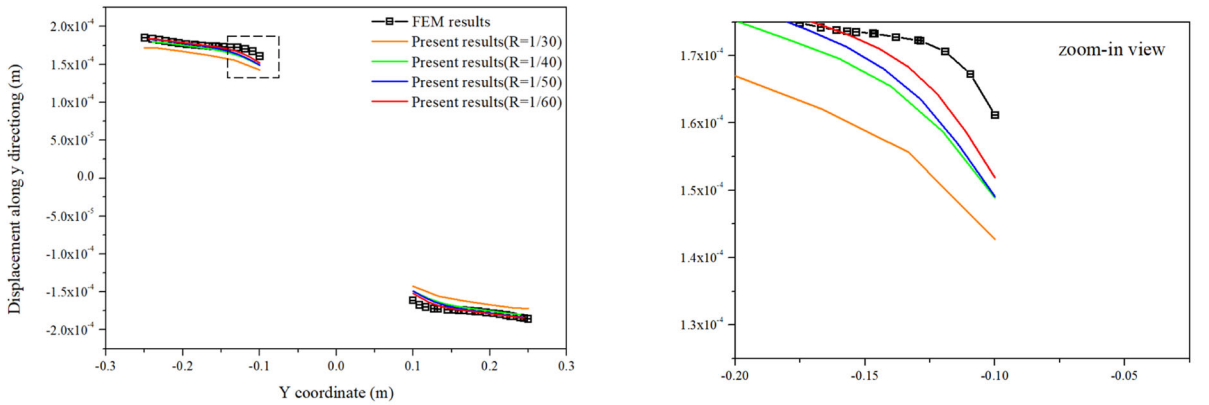

(b) Vertical displacement

Fig. 9 The distribution of displacements along horizontal and vertical central lines

3.1 Elastic problems in three-dimensional case

The elastic problems in three-dimensional cases are examined in this subsection. As shown in Fig. 6, a rectangular block without a hole and a rectangular block with a hole in the center are utilized.

A rectangular block without a hole is used to verify the Poisson's ratio of the proposed model. The loading conditions and geometric dimensions of this rectangular block are plotted in Fig. 6a. The uniform tensile loads of 200MPa are applied to the right boundary in the x direction, and the left boundary is fixed. The rectangular block is discretized into $100 \times 50 \times 50$ cubic lattices, and inner diameter of each cubic lattice is 20 mm. The mechanical parameters are as follows: Young's modulus $E = 2.0 \times 10^{11}$Pa, density $\rho = 7850\text{kg/m}^3$. Poisson's ratio v is varied in simulation. As shown in Fig. 7, the results obtained by the proposed model are compared with those obtained by classical lattice model and theoretical solutions at different Poisson' ratio. It is found from Fig. 7 that the results obtained by the proposed model are in good agreement with theoretical solutions, while the results obtained by classical lattice models are not consistent with theoretical solutions. This implies that the proposed model can consider varied Poisson's ratios. Moreover, as shown in Fig. 8, the results obtained by the proposed model are compared with those obtained by FEM at v=0.15. It is found from Fig. 8 that the results obtained by the proposed model are in good agreement with FEM solution, implying the proposed model can consider three-dimensional elastic problems.

A rectangular block with a hole in the center is utilized to investigate the convergence of the proposed model. The loading conditions and geometric

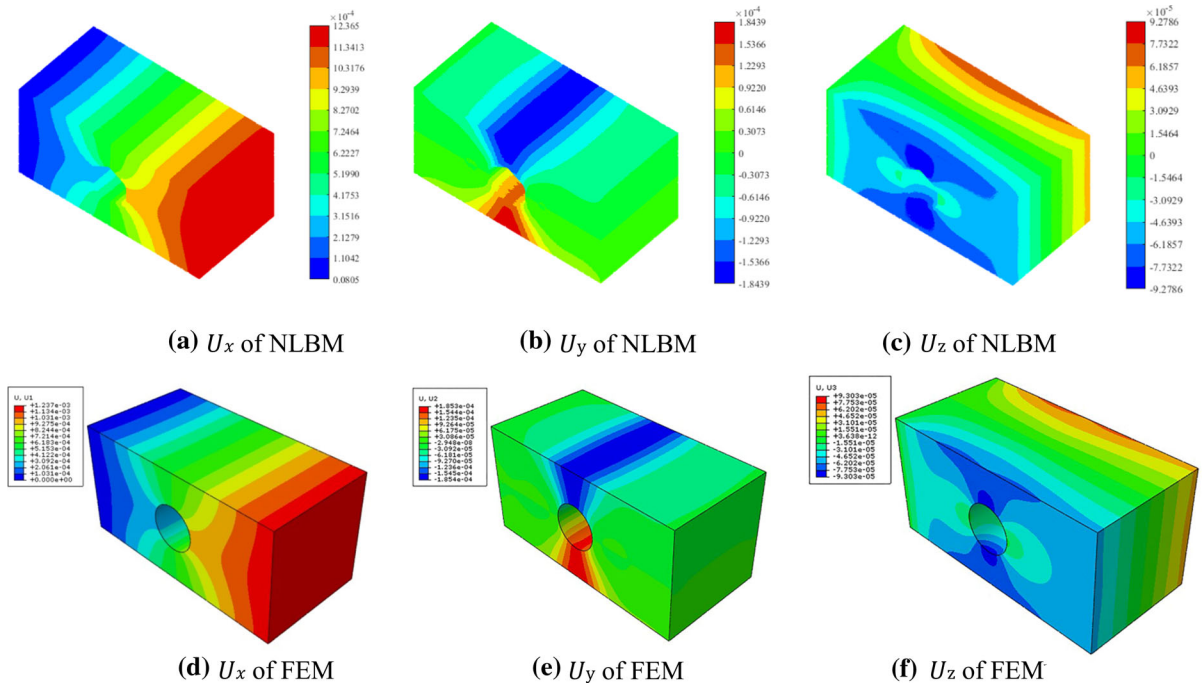

Fig. 10 Displacement contours of block with a hole

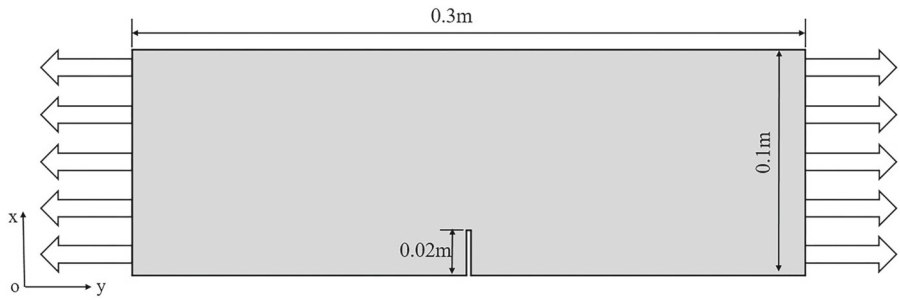

Fig. 11 The configuration of the plate with a single-edge notch

dimensions of this rectangular block with a hole are plotted in Fig. 6b. The uniform tensile loads of 200 MPa are applied to the right boundary in the x direction, and the left boundary is fixed. The rectangular block is discretized into 100 × 50 × 50 cubic lattices, while inner diameter of each cubic lattice is varied. The mechanical parameters are as follows: Young's modulus E = 2.0×10^{11}Pa, Poisson's ratio $v = 0.2$ and density $\rho = 7850\text{kg/m}^3$. As shown in Figs. 9 and 10, the numerical results of the proposed model with v=0.2 are compared with those obtained by FEM. It is found from Fig. 9 that the results obtained by the proposed model are more consistent with the FEM results as inner diameter of each cubic lattice decreases. In other words, the results obtained by the proposed model are more consistent with the FEM results as the number of lattices increases.

3.2 Fracture problems in two-dimensional case

After verifying the validity of the proposed model for the elastic problems, fracture problems in two-dimensional cases are conducted. The loading conditions and geometric dimensions of this plate with a single-edge notch are shown in Fig. 11. The velocity of 0.002 mm/step is applied to the upper and the lower edges in the y direction. The plate with a single-edge-notched is discretized into 100 × 300 square lattices. The mechanical parameters are as follows: Young's modulus E = 69×10^9Pa, density $\rho = 2700\text{kg/m}^3$,

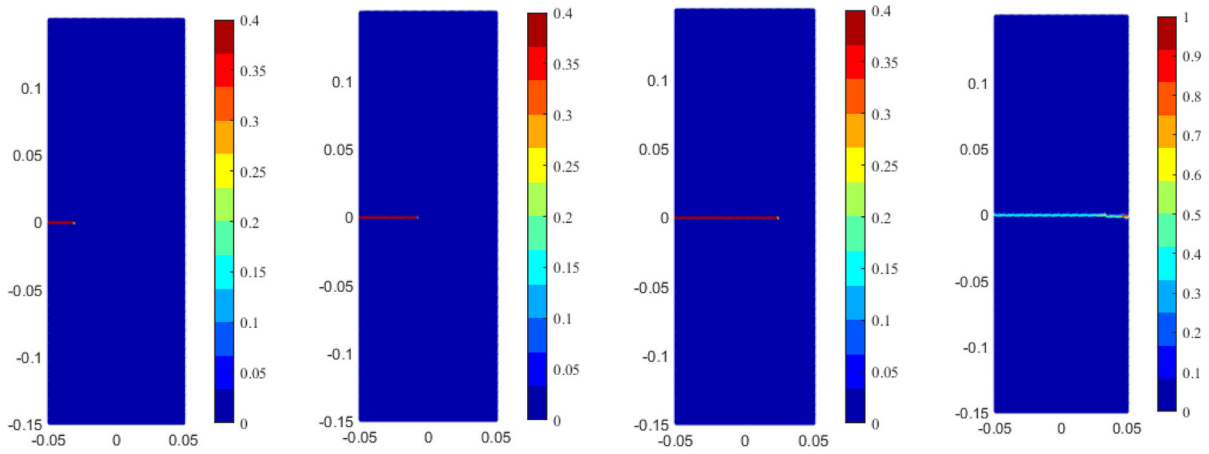

(a) Step 100 **(b)** Step 26000 **(c)** Step 26400 **(d)** Step 27000

Fig. 12 The crack evolution in two-dimensional case

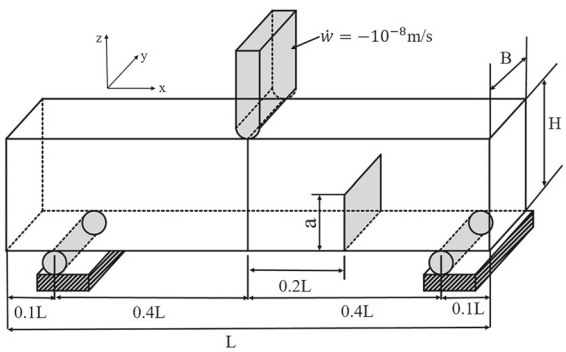

Fig. 13 The configuration of the block with a single-edge notch

Poisson's ratio $v = 0.3$ and the critical bond energy potential w_{2D}^0 =6.07 mJ/mm^6.

As illustrated in Fig. 12, the new crack initiates from the tip of the single-edge-notch and propagates along the pre-existing crack direction until the failure of the rectangle plate occurs. The results obtained by the proposed model are in good agreement with those obtained by the Linear Elastic Fracture Mechanics, in which the crack propagates along its original crack plane (i.e., pure mode I) until the specimen failure occurs (Chen et al. 2014).

3.3 Fracture problems in three-dimensional case

In this subsection, the fracture problems in three-dimensional cases are investigated. The loading conditions and geometric dimensions of this block with a single-edge-notch are shown in Fig. 13. Based on the work by Jenq and Shah (1988), the dimensions (L × B × H) of the single-edge notched block are 304.8 mm × 28.6 mm × 70.2 mm and the height of the notch is 35.1 mm. The velocity of 1×10^{-5} mm/step is applied to the upper edge in the opposite direction of the z axis. The block with a single-edge-notched is discretized into 202 × 20 × 48 cubic lattices. The mechanical parameters are as follows: Young's modulus E = 30×10^9Pa, density $\rho = 3000\text{kg/m}^3$, Poisson's ratio $v = 0.2$ and the critical energy release rate G_c=20.7368 J/m^2.

As shown in Fig. 14, the new crack initiates from the tip of the pre-existing flaw and propagates to the middle of the beam until the beam fails. The results obtained by the proposed model show that the failure angle is β=28°, which are in good agreement with the failure angle observed in experiments (Nguyen and Oterkus 2020).

3.4 Fracture behaviors in brittle solids

After verifying the validity of the proposed model for the two-dimensional and three-dimensional fracture problems, fracture behavior prediction in brittle solids is conducted in this subsection. The elongation at break of PMMA is 2–3%. As a result, the diagonally loaded square PMMA plate is chosen to study the fracture behavior prediction in brittle solids. The loading conditions and geometric dimensions of this diagonally loaded square plate are shown in Fig. 15. Based on the work by Ayatollahi and Aliha (2009), the

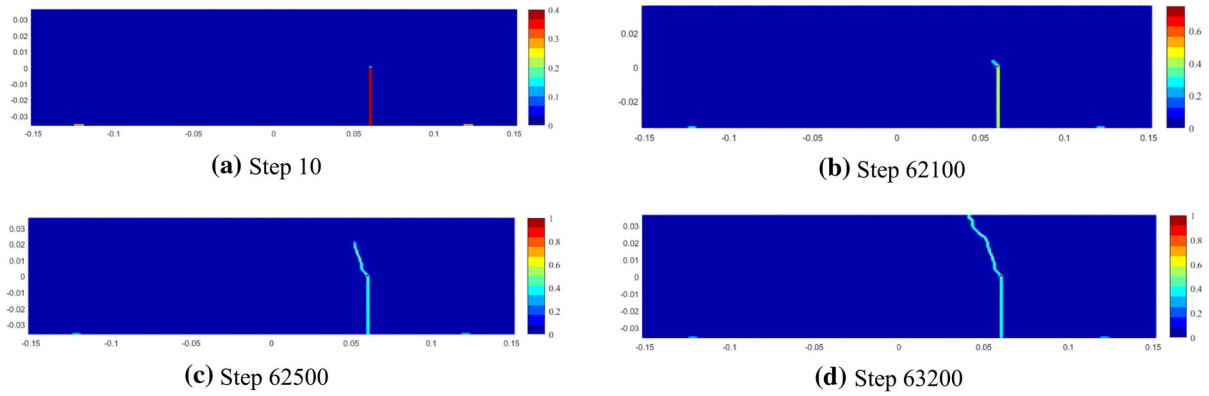

Fig. 14 The crack evolution in three-dimensional case

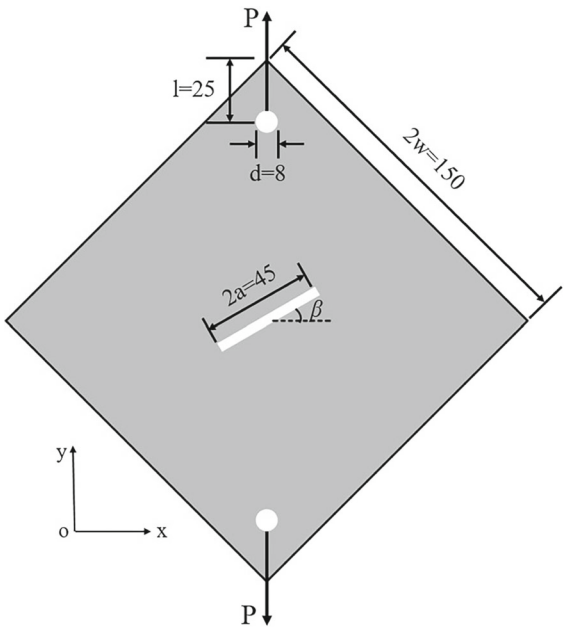

Fig. 15 The configuration of the diagonally loaded square plate (Unit: mm)

dimensions of the diagonally loaded square plate are 150 mm × 150 mm × 5 mm. The velocity of 0.17×10^{-5} mm/step is applied to the lattices confined to the two hole in the y direction. The diagonally loaded square plate is discretized into 150 × 150 squares lattices. The mechanical parameters are as follows: Young's modulus E = 2940×10^6Pa, density $\rho = 1180\text{kg/m}^3$, Poisson's ratio $v = 0.3$ and the critical energy release rate G_c=601.7 J/m^2. The crack length is 2a = 45 mm, and the varying crack angles are β=0°, 15°, 30°, 45° and 62.5°.

As illustrated in Fig. 16, the fracture behaviors for various initial crack angles in brittle solids observed by the proposed model are compared with other numerical results (Guo 2019) and experimental observations (Ayatollahi and Aliha 2009). The final crack paths for all pre-existing cracks predicted by the proposed model are vertical to the tensile stress direction. Compared with the previous numerical results, i.e. the peridynamic lattice model (PDLM), the proposed model (NLBM) has better performance, which is more consistent with the experimental observation. The predicted failure loads are also compared with the previous numerical results and experimental measurements. The failure loads predicted by the proposed model are in good agreement with those obtained by the previous numerical method and experiments, as shown in Fig. 17.

4 Conclusions

A three-dimensional non-local lattice bond model (NLBM) is proposed to predict the fracturing behaviors in brittle solids. In the proposed model, the nonlocal interaction terms, i.e. the tangential bonds, are adopted to overcome the fixed Poisson's ratio limitation. The stiffness parameters for three-dimensional non-local lattice bond model are obtained by comparing the strain energy stored in a discrete unit lattice with the classical continuum strain energy. The capabilities of the three-dimensional non-local lattice bond model are demonstrated using various benchmarks including elastic problems and fracture problems, and the results obtained by the proposed model

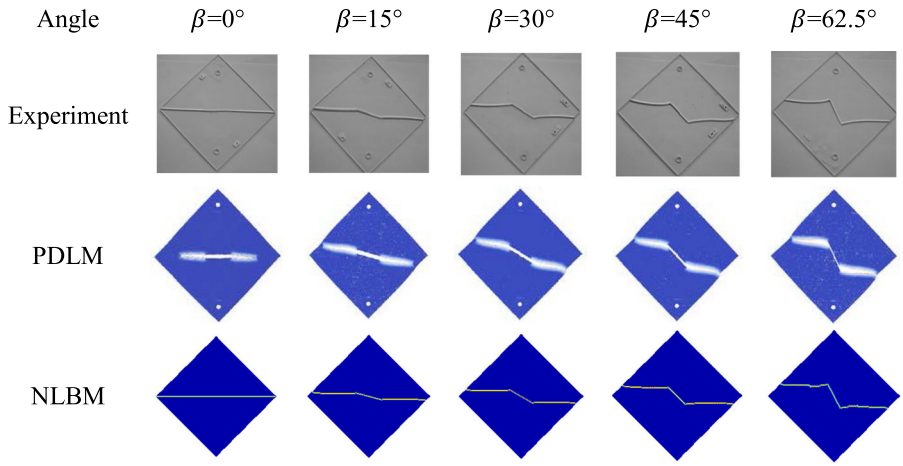

Fig. 16 The fracture behaviors in brittle solids

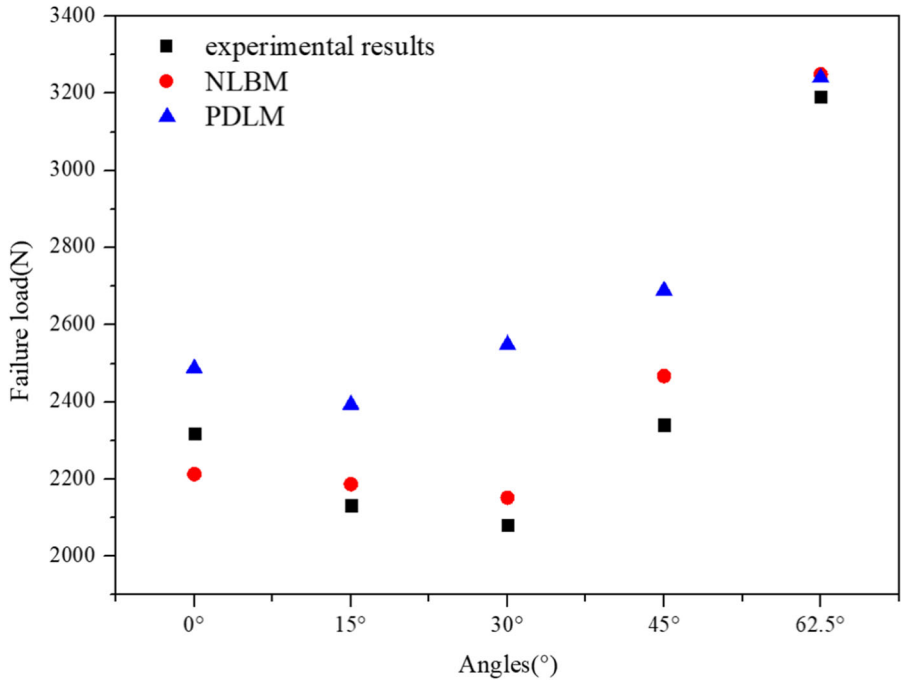

Fig. 17 Comparison of experimental and numerical failure loads

are compared with those obtained by the previous numerical results and experiments. In three-dimensional non-local lattice bond model, no additional crack extension criterion is required, and it is illustrated that the proposed model has better capabilities to predict the fracturing behaviors of brittle solids with varied crack angles.

Acknowledgements This work was supported by the National Natural Science Foundation of China (Grant Nos. 51839009 and 52027814) and the Graduate Scientific Research and Innovation Foundation of Chongqing, China (Grant No. CYB20033).

References

Ayatollahi MR, Aliha MRM (2009) Analysis of a new specimen for mixed mode fracture tests on brittle materials. Eng Fract Mech 76(11):1563–1573

Belytschko T, Gracie R, Ventura G (2009) A review of extended/generalized finite element methods for material modeling. Model Simul Mater Sci 17(4):043001

Caldarelli G, Castellano C, Petri A (1999) Criticality in models for fracture in disordered media. Physica A 270(1):15–20

Chen KT, Wu JH (2018) Simulating the failure process of the Xinmo landslide using discontinuous deformation analysis. Eng Geol 239:269–281

Chen HL, Lin EQ, Jiao Y, Liu YM (2014) A generalized 2D non-local lattice spring model for fracture simulation. Comput Mech 54:1541–1558

Cundall PA, Strack ODL (1979) A discrete numerical model for granular assemblies. Geotechnique 29(1):47–65

Cusatis G, Bažant ZP, Cedolin L (2003) Confinement-shear lattice model for concrete damage in tension and compression: I. Theory. J Eng Mech-ASCE 129(12):1439–1448

Grassl P, Bazant ZP, Cusatis G (2006) Lattice-cell approach to quasi-brittle fracture modeling. Computational Modelling of Concrete Structures: Proceedings of the EURO-C conference 2006, in Mayrhofen, Tyrol, Austria

Griffiths DV, Mustoe GGW (2001) Modelling of elastic continua using a grillage of structural elements based on discrete element concepts. Int J Numer Meth Eng 50:1759–1775

Guo J (2019) Research on peridynamic lattice model and its applications on dynamic brittle fracture modeling. Harbin Institute of Technology

Hrennikoff A (1941) Solution of problems of elasticity by the framework method. J Appl Mech 18:169–175

Jenq YS, Shah SP (1988) Mixed-mode fracture of concrete. Int J Fract 38(2):123–142

Kawai T (1978) New discrete models and their application to seismic response analysis of structures. Nucl Eng Des 48(1):207–229

Lilliu G, van Mier JGM (2003) 3D lattice type fracture model for concrete. Eng Fract Mech 70:927–941

Madenci E, Oterkus E (2014) Peridynamic theory and its applications. Springer, Boston

Nguyen CT, Oterkus S (2020) Ordinary state-based peridynamic model for geometrically nonlinear analysis. Eng Fract Mech 224:106750

Ostoja-Starzewski M (2002) Lattice models in micromechanics. Appl Mech Rev 55(1):35–60

Silling SA, Askari E (2005) A meshfree method based on the peridynamic model of solid mechanics. Comput Struct 83:1526–1535

Silling SA, Epton E, Weckne O, Xu J (2007) Peridynamic states and constitutive modeling. J Elast 88:151–184

Wang YT, Zhou XP, Kou MM (2018a) A coupled thermo-mechanical bond-based peridynamics for simulating thermal cracking in rocks. Int J Fract 211(1–2):13–42

Wang YT, Zhou XP, Wang Y, Shou YD (2018b) A 3-D conjugated bond-pair-based peridynamic formulation for initiation and propagation of cracks in brittle solids. Int J Solids Struct 134:89–115

Yang YT, Tang XH, Zheng H, Liu QS, He L (2016) Three-dimensional fracture propagation with numerical manifold method. Eng Anal Bound Elem 72:65–77

Yu HJ, Sumigawa T, Wu LZ, Kitamura T (2015) Generalized domain-independent interaction integral for solving the stress intensity factors of nonhomogeneous materials. Int J Solids Struct 67–68:151–168

Zeng W, Liu GR, Kitamura Y, Nguyen-Xuan H (2013) A three-dimensional ES-FEM for fracture mechanics problems in elastic solids. Eng Fract Mech 114:127–150

Zhang ZN, Ge XR (2006) Micromechanical modelling of elastic continuum with virtual multi-dimensional internal bonds. Int J Numer Meth Engng 65:135–146

Zhang ZN, Ge XR (2007) Multiscale shear fracture of heterogeneous material using the virtual internal bond. Theor Appl Frac 47:185–191

Zhao GF (2017) Developing a four-dimensional lattice spring model for mechanical responses of solids. Comput Method Appl M 315:881–895

Zhao GF, Deng ZQ, Zhang B (2019) Multibody failure criterion for the four-dimensional lattice spring model. Int J Rock Mech Min 123:104126

Zhou XP, Shou YD (2016) Numerical simulation of failure of rock-like material subjected to compressive loads using improved peridynamic method. Int J Geomech 17(3):04016086

Zhou XP, Zhang JZ, Wong LNY (2018) Experimental study on the growth, coalescence and wrapping behaviors of 3D cross-embedded flaws under uniaxial compression. Rock Mech Rock Eng 51(5):1379–1400

Zhou XP, Chen JW, Berto F (2020a) XFEM based node scheme for the frictional contact crack problem. Comput Struct 231:106221

Zhou XP, Wang LF, Shou YD (2020b) Understanding the fracture mechanism of ring Brazilian disc specimens by the phase field method. Int J Fract 226(1):17–43

Zhou XP, Fu L, Qian QH (2021) A 2D novel non-local lattice bond model for initiation and propagation of cracks in rock materials. Eng Anal Bound Elem 126:181–199

Zienkiewicz OC, Taylor RL (2000) The finite element method, 5th edn. Butterworth-Heinemann, Oxford

Zubelewicz A, Bažant Z (1987) Interface element modeling of fracture in aggregate composites. J Eng Mech 113(11):1619–1630